Pergamon

Geochimica et Cosmochimica Acta, Vol. 67, No. 9, pp. 1667–1676, 2003

0016-7037/03 $30.00 + .00

doi:10.1016/S0016-7037(02)01275-9

Influence of lysozyme on the precipitation of calcium carbonate: A kinetic and morphologic study

CONCEPCION JIMENEZ-LOPEZ,[2] ALEJANDRO RODRIGUEZ-NAVARRO,[1,*] JOSE M. DOMINGUEZ-VERA,[3] and JUAN M. GARCIA-RUIZ[1]

[1]Instituto Andaluz de Ciencias de la Tierra, CSIC-Universidad de Granada, Campus de Fuentenueva, 18002 Granada, Spain
[2]Estacion Experimental del Zaidin-CSIC, C/Prof. Albareda, 1, 18008 Granada, Spain
[3]Departmento de Química Inorgánica, Facultad de Ciencias, Universidad de Granada, 18002 Granada, Spain

(*Received October* 22, 2001; *accepted in revised form August* 30, 2002)

Abstract—Several mechanisms have been proposed to explain the interactions between proteins and mineral surfaces, among them a combination of electrostatic, stereochemical interactions and molecular recognition between the protein and the crystal surface. To identify the mechanisms of interaction in the lysozyme–calcium carbonate model system, the effect of this protein on the precipitation kinetics and morphology of calcite crystals was examined. The solution chemistry and morphology of the solid were monitored over time in a set of time-series free-drift experiments in which $CaCO_3$ was precipitated from solution in a closed system at 25°C and 1 atm total pressure, in the presence and absence of lysozyme. The precipitation of calcite was preceded by the precipitation of a metastable phase that later dissolved and gave rise to calcite as the sole phase. With increasing lysozyme concentration, the nucleation of both the metastable phase and calcite occurred at lower $\Omega_{calcite}$, indicating that lysozyme favored the nucleation of both phases. Calcite growth rate was not affected by the presence of lysozyme, at least at protein concentrations ranging from 0 mg/mL to 10 mg/mL.

Lysozyme modified the habit of calcite crystals. The degree of habit modification changed with protein concentration. At lower concentrations of lysozyme, the typical rhombohedral habit of calcite crystals was modified by the expression of {110} faces, which resulted from the preferential adsorption of protein on these faces. With increasing lysozyme concentration, the growth of {110}, {100}, and finally {001} faces was sequentially inhibited. This adsorption sequence may be explained by an electrostatic interaction between lysozyme and calcite, in which the inhibition of the growth of {110}, {100}, and {001} faces could be explained by a combined effect of the density of carbonate groups in the calcite face and the specific orientation (perpendicular) of these carbonate groups with respect to the calcite surface. Overgrowth of calcite in the presence of lysozyme demonstrated that the protein favored and controlled the nucleation on the calcite substrate. Overgrowth crystals nucleated epitaxially in lines which run diagonal to rhombohedral {104} faces.

1. INTRODUCTION

Organisms induce the precipitation of a large variety of minerals (Lowenstand, 1981). Some of them form mineralized tissues with extremely sophisticated shapes and highly organized microstructures (i.e., mollusk shells, coccoliths) (Mann et al., 1989; Simkiss and Wilbur, 1989; Checa and Rodriguez-Navarro, 2001). From the study of these materials it is apparent that organisms are able to control the nucleation, size, morphology, and crystallographic orientation of crystals (Addadi and Weiner, 1992). Despite the extensive research on the subject, the mechanisms involved in these complex mineralization processes are poorly understood. However, there is evidence from in vitro experiments that the interaction of proteins with minerals plays an important role in controlling biomineralization (Lowenstand and Weiner, 1989; Nys et al., 1999). Proteins can promote or inhibit the nucleation of crystals and can also control their morphology (Lowenstand and Weiner, 1989; Wheeler et al., 1981; Mann et al., 1990). It has been suggested that proteins also control polymorphism (e.g., precipitation of calcite or aragonite; Falini et al., 1995; Belcher et al., 1996). Several mechanisms have been proposed to explain the interactions between proteins and mineral surfaces, among them a combination of electrostatic and stereochemical interactions, as well as geometrical matching. This geometrical matching implies that the arrangement of the functional groups in the macromolecule matches that of the ionic groups in the crystal plane (Addadi et al., 1987; Mann, 1988). To understand these mechanisms, it would be convenient to study them separately using systems in which only one kind of interaction would be predominant (Rodriguez-Navarro et al., 2000). Whether one kind of interaction is predominant will depend on the size, conformation, and other properties of the molecules (e.g., charge, type of functional groups). For instance, Langmuir monolayers made of small molecules (e.g., surfactants) can induce the nucleation of crystals on specific crystal planes to which they bind at specific sites (Heywood, 1996). In this case the predominant interaction is a geometrical matching between the arrangement of the molecules and the surface of the crystal. On the other hand, in a previous study we examined (Rodriguez-Navarro et al., 2000) the interaction between the calcite surfaces and a group of globular proteins (lysozyme, ribonuclease, myoglobin, and α-lactalbumin) of similar size and conformation (three-dimensional [3-D] molecular structure), but different in their surface charges (Arai and Norde, 1990; Haynes and Norde, 1994). In addition, the relatively large size of these proteins precludes an arrangement that

* Author to whom correspondence should be addressed (anava@ugr.es).

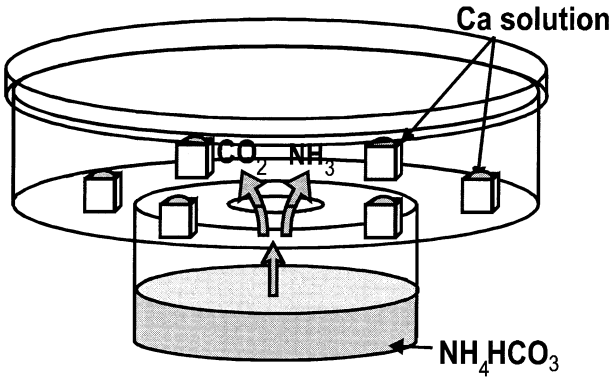

Fig. 1. Experimental setup. Calcite crystals were grown in sitting droplets on microbridges. $NH_{3(g)}$ and $CO_{2(g)}$ slowly diffused from the reservoir to the droplet through the small opening in the Petri plate.

would match the crystal surface geometry at the atomic level. The dominant mechanism governing this interaction was the adsorption of proteins onto specific calcite faces to which they were electrostatically attracted. As a continuation of this research, the present paper is a detailed examination of how one of these proteins (lysozyme) affects the precipitation kinetics of calcium carbonate and calcite crystal growth morphology.

2. EXPERIMENTAL METHODS

2.1. Materials

Certified chemical reagents (Sigma) were used to prepare stock solutions of $CaCl_2$ (0.4 mol/L), lysozyme (100 mg/mL), and NH_4HCO_3 (0.025 mol/L).

2.2. Precipitation System

The precipitation experiments were carried out at 25°C and 1 atm total pressure in 12 isolated environmental chambers, specially designed for these experiments. Each chamber consisted of a glass Petri dish (2×10 cm diameter) containing six microbridges (for sitting drop crystallization; Crystal Microsystems) with $CaCl_2$/lysozyme solution (master solution). This Petri dish was placed on top of a cylindrical vessel 5 cm in diameter and 3 cm in height containing the NH_4HCO_3 solution and connected to the Petri dish by a hole (Fig. 1). The empty space contained inside the system (cylindrical vessel and Petri dish) is referred to here as free-space with a volume of 153.678 mL.

2.3. Calcite Nucleation and Growth in the Presence of Lysozyme

Free drift precipitation experiments were performed in the absence of lysozyme (control experiment) using pure $CaCl_2$ (0.25 mol/L) as master solution and in the presence of lysozyme at different concentrations (0.1, 1, 10, 25, and 50 mg/mL). In the lysozyme-bearing experiments, the concentration of the $CaCl_2$ solution was kept constant at 0.25 mol/L, while varying concentrations of lysozyme. The resulting master solutions in the lysozyme-bearing experiments were as follows: $CaCl_2$ (0.25 mol/L)/lysozyme (0.1 mg/mL), $CaCl_2$ (0.25 mol/L)/lysozyme (10 mg/mL), $CaCl_2$ (0.25 mol/L)/lysozyme (25 mg/mL), and $CaCl_2$ (0.25 mol/L)/lysozyme (50 mg/mL). To begin a run, a drop of 40 μL of the master solution was poured on each microbridge already placed inside the Petri dish. A volume of 3 mL of the NH_4HCO_3 solution was poured into the underlying cylindrical vessel. The system was then closed and sealed with silicon grease (Fig. 1). The underlying NH_4HCO_3 solution released $NH_{3(g)}$ and $CO_{2(g)}$ into the free-space in the chamber according to the following equilibrium reactions:

$$NH^+_{4(aq)} + OH^- \Leftrightarrow NH_{3(aq)} + H_2O \Leftrightarrow NH_{3(g)}$$

and

$$HCO^-_{3(aq)} + H^+ \Leftrightarrow CO_{2(aq)} + H_2O \Leftrightarrow CO_{2(g)} + H_2O_{(l)}$$

The $NH_{3(g)}$ then redissolved into the master solution and increased the pH to maintain equilibrium in the system. The $CO_{2(g)}$ redissolved into the master solution as well, thus producing $CO_{2(aq)}$, $HCO^-_{3\,(aq)}$, and $CO^{2-}_{3\,(aq)}$.

A set of time-series experiments was run for each one of the master solutions. Twelve replicas of the same experiment were run in parallel. Each replica was terminated at different times (0, 0.5, 1, 1.5, 2, 2.5, 3, 3.5, 4, 5, 7, or 7.5 and 9 h after sealing the system), and both solution and solid were withdrawn from the microbridges for chemical and morphologic analyses. Long-term experiments were run for 19.5, 27.5, and 52.5 h (after sealing the system), and the solid phase was recovered to study the crystal morphology.

2.4. Overgrowth of Calcite Crystals in the Presence of Lysozyme

To study the effect of the protein on the overgrowth of calcite substrates, rhombohedral calcite crystals selected from the control experiments (lysozyme-free) were used as substrates. To begin a run, a drop of 40 μL of the master solution and two rhombohedral calcite crystals (collected from the control experiment) were placed on each microbridge. Three mL of the NH_4HCO_3 solution were poured into the underlying cylindrical vessel. The system was then closed and sealed with silicon grease (Fig. 1). A set of time-series experiments was run for each one of the above-mentioned master solutions. Seven replicas of the same experiment were run in parallel. Each replica was terminated at different times (0, 0.5, 1.5, 4.5, 17, 25, and 50 h after sealing the system), and the overgrown calcite crystals were harvested from the microbridges.

2.5. Analytical Procedures

Solution pH was measured using a micro-electrode (PHR-146, Lazar) after calibration with standard buffer solutions for temperature and slope correction. To measure the pH while maintaining the system sealed, the microelectrode was introduced into a hole made in the lid covering the Petri dish. Total calcium concentration in solution ($Ca^{2+}_{T(aq)}$) was determined by atomic absorption spectrophotometry (AAS, Perkin-Elmer 5100) using an air–acetylene flame atomizer after acidification of filtered samples with HCl to prevent the precipitation of solid carbonate. Experimental error for $Ca^{2+}_{T(aq)}$ was ± 0.006 mol/L (1σ). The concentration of lysozyme of the master solution was measured using an ultraviolet-visible spectrometer at 280 μm. The time at which the first precipitate was observed in the microbridges (referred to here as waiting time for precipitation), the number and size of crystals, and the presence or absence of an amorphous phase were all determined using an optical microscope (SZH10 Olympus, 14×). The precipitate was harvested from the microbridges, rinsed twice with Milli-Q water, dried at room temperature, coated with gold, and observed with a scanning electron microscope (SEM, DMS 950 Zeiss).

2.6. Speciation Calculations

The speciation program EQ3/6 (Wolery, 1992) was used to calculate the fugacity for $NH_{3(g)}$ and $CO_{2(g)}$ in equilibrium with the NH_4HCO_3 solution (0.025 mol/L) at a measured pH of 7.80. The resulting fugacity for $NH_{3(g)}$ was 1.05×10^{-5} bars and for $CO_{2(g)}$ was 2.34×10^{-2} bars. However, the carbon moles necessary to create such $CO_{2(g)}$ fugacity in the free-space exceeded the carbon moles available in the system. The actual $CO_{2(g)}$ fugacity in the free-space, in equilibrium with the master solution at each time interval, was calculated by iteration. Iteration was performed on the basis of the following: 1) maximum moles of carbon available in the system at each time interval, 2) the ideal gas equation, 3) distribution of carbon moles between gas and solution phases, and 4) the equilibrium equation for total dissolved inorganic carbon in solution (ΣCO_2) and $P_{CO2(g)}$ at the pH of the master solution at each time interval (Morse and Mackenzie, 1990). The fugacity coefficient was

Table 1. Measured pH and total calcium concentration in solution, $Ca^{2+}{}_{T(aq)}$. Calculated fugacity (f) of $CO_{2(g)}$, activities (a) of carbonate species, $Ca^{2+}{}_{(aq)}$ and Ca-species, supersaturation with respect to calcite and calcite growth rate.

Lysozyme (mg/mL)	Time (h)	pH	$Ca^{2+}{}_{T(aq)}$ (M)	$f_{CO2(g)}$ (atm)	$aHCO^{-}_{3(aq)}$ (M)	$aCO^{2-}_{3(aq)}$ (M)	$aCa^{2+}_{(aq)}$ (M)	$aCaOH^{+}_{(aq)}$ (M)	$aCaHCO^{+}_{3(aq)}$ (M)	$aCaCO^{0}_{3(aq)}$ (M)	$\Omega_{calcite}$	SA (m^2/g)	ln r (mol/m^2h)
0	0	5.04	0.252	1.93E-03	4.45E-06	1.15E-11	4.19E-02	8.62E-11	2.40E-06	8.04E-10	0		
0	0.5	7.68	0.251	1.93E-03	1.94E-03	2.18E-06	4.19E-02	3.77E-08	1.05E-03	1.53E-04	22		
0	1	8.31	0.230	1.93E-03	8.28E-03	3.98E-05	4.10E-02	1.57E-07	4.37E-03	2.73E-03	392		
0	1.5	8.55	0.215	1.79E-03	1.33E-02	1.35E-04	4.02E-02	2.68E-07	6.90E-03	9.08E-03	1076		
0	2	8.54	0.237	1.71E-03	1.25E-02	1.02E-04	4.13E-02	2.69E-07	6.62E-03	7.03E-03	1009		
0	2.5	8.66	0.244	1.85E-03	1.78E-02	1.79E-04	4.14E-02	3.56E-07	9.47E-03	1.24E-02	1903	0.11	
0	3	8.71	0.248	1.89E-03	2.04E-02	2.46E-04	4.15E-02	4.00E-07	1.09E-02	1.71E-02	2451	0.07	
0	3.5	8.73	0.231	1.92E-03	2.17E-02	2.74E-04	4.06E-02	4.09E-07	1.13E-02	1.86E-02	2671	0.06	3.73
0	4	8.73	0.211	1.80E-03	2.03E-02	2.57E-04	3.96E-02	3.99E-07	1.03E-02	1.70E-02	2441	0.06	3.11
0	5	8.73	0.201	1.69E-03	1.91E-02	2.41E-04	3.90E-02	3.93E-07	9.57E-03	1.57E-02	2258	0.05	2.25
0	7	8.73	0.209	1.63E-03	1.84E-02	2.32E-04	3.95E-02	3.98E-07	9.35E-03	1.54E-02	2207	0.04	
0	9	8.73	0.206	1.67E-03	1.88E-02	2.38E-04	3.92E-02	3.96E-07	9.52E-03	1.56E-02	2246	0.04	1.59
0.1	0	4.12	0.254	1.93E-03	5.35E-07	1.66E-13	4.20E-02	1.04E-11	2.89E-07	1.15E-11	0		
0.1	0.5	7.37	0.249	1.93E-03	9.50E-04	5.24E-07	4.18E-02	1.84E-08	5.12E-04	3.64E-05	5		
0.1	1	8.01	0.250	1.91E-03	4.11E-03	9.88E-06	4.19E-02	8.06E-08	2.22E-03	6.87E-04	100		
0.1	1.5	8.27	0.241	1.91E-03	7.47E-03	3.27E-05	4.16E-02	1.45E-07	4.00E-03	2.26E-03	327		
0.1	2	8.43	0.242	1.85E-03	1.05E-02	6.62E-05	4.16E-02	2.10E-07	5.60E-03	4.57E-03	662		
0.1	2.5	8.53	0.250	1.85E-03	1.32E-02	1.05E-04	4.19E-02	2.66E-07	7.10E-03	7.29E-03	1057	0.22	
0.1	3	8.60	0.240	1.91E-03	1.60E-02	1.50E-04	4.13E-02	3.09E-07	8.50E-03	1.03E-02	1487	0.15	2.91
0.1	3.5	8.66	0.234	1.85E-03	1.78E-02	1.91E-04	4.10E-02	3.52E-07	9.38E-03	1.30E-02	1883	0.11	2.35
0.1	4	8.70	0.221	1.80E-03	1.90E-02	2.23E-04	4.02E-02	3.79E-07	9.82E-03	1.49E-02	2162	0.09	2.67
0.1	5	8.76	0.232	1.73E-03	2.09E-02	2.83E-04	4.06E-02	4.39E-07	1.09E-02	1.91E-02	2767	0.07	
0.1	7	8.76	0.235	1.80E-03	2.18E-02	2.94E-04	4.08E-02	4.41E-07	1.14E-02	1.99E-02	2888	0.07	
0.1	9	8.76	0.229	1.80E-03	2.18E-02	2.94E-04	4.05E-02	4.37E-07	1.13E-02	1.98E-02	2866	0.07	1.91
10	0	4.10	0.246	1.93E-03	5.10E-07	1.51E-13	4.16E-02	9.85E-12	2.74E-07	1.04E-11	0		
10	0.5	7.34	0.246	1.93E-03	8.87E-04	4.56E-07	4.17E-02	1.71E-08	4.76E-04	3.16E-05	5		
10	1	7.78	0.236	1.93E-03	2.44E-03	3.46E-06	3.44E-02	3.90E-08	1.08E-03	1.98E-04	29		
10	1.5	8.22	0.176	1.87E-03	6.50E-03	2.54E-05	3.05E-02	9.48E-08	2.55E-03	1.28E-03	186		
10	2	8.46	0.230	1.51E-03	9.11E-03	6.18E-05	3.41E-02	1.84E-07	4.00E-03	3.50E-03	507		
10	2.5	8.60	0.225	1.84E-03	1.54E-02	1.44E-04	4.06E-02	3.04E-07	8.05E-03	9.71E-03	1407	0.07	
10	3	8.69	0.195	1.80E-03	1.85E-02	2.13E-04	3.87E-02	3.56E-07	9.22E-03	1.37E-02	1986	0.04	3.19
10	3.5	8.70	0.187	1.62E-03	1.65E-02	1.95E-04	3.81E-02	3.59E-07	8.13E-03	1.23E-02	1789	0.03	2.46
10	4	8.70	0.202	1.57E-03	1.65E-02	1.95E-04	3.92E-02	3.69E-07	8.34E-03	1.27E-02	1836	0.03	
10	5	8.73	0.205	1.67E-03	1.88E-02	2.38E-04	3.92E-02	3.96E-07	9.52E-03	1.55E-02	2246	0.03	
10	7.5	8.73	0.204	1.69E-03	1.91E-02	2.41E-04	3.92E-02	3.95E-07	9.62E-03	1.57E-02	2269	0.02	1.34
10	9	8.73	0.207	1.67E-03	1.88E-02	2.38E-04	3.93E-02	3.97E-07	9.55E-03	1.55E-02	2253	0.02	
50	0	4.40	0.252	1.93E-03	1.02E-06	6.02E-13	4.19E-02	1.98E-11	5.49E-07	4.18E-11	0		
50	0.5	6.12	0.252	1.93E-03	5.35E-05	1.66E-09	4.19E-02	1.04E-09	2.88E-05	1.15E-07	0		
50	1	7.03	0.248	1.93E-03	4.34E-04	1.10E-07	4.18E-02	8.41E-09	2.34E-04	7.59E-06	1		
50	1.5	7.74	0.246	1.92E-03	2.22E-03	2.87E-06	4.17E-02	4.31E-08	1.19E-03	1.98E-04	29		
50	2	8.20	0.247	1.90E-03	6.33E-03	2.36E-05	4.18E-02	1.25E-07	3.41E-03	1.64E-03	237		
50	2.5	8.36	0.246	1.92E-03	9.24E-03	4.98E-05	4.17E-02	1.80E-07	4.97E-03	3.45E-03	500		
50	3	8.44	0.194	1.90E-03	1.10E-02	7.12E-05	3.90E-02	2.02E-07	5.53E-03	4.61E-03	669		
50	3.5	8.48	0.187	1.58E-03	1.00E-02	7.12E-05	3.85E-02	2.19E-07	4.98E-03	4.55E-03	660		
50	4	8.56	0.177	1.54E-03	1.18E-02	1.00E-04	3.77E-02	2.57E-07	5.71E-03	6.29E-03	911		
50	5	8.59	0.179	1.48E-03	1.21E-02	1.11E-04	3.79E-02	2.77E-07	5.91E-03	6.96E-03	1010		
50	7.5	8.56	0.183	1.49E-03	1.14E-02	9.71E-05	3.82E-02	2.61E-07	5.60E-03	6.16E-03	894	0.03	
50	9	8.51	0.182	1.51E-03	1.03E-02	7.82E-05	3.82E-02	2.32E-07	5.05E-03	4.95E-03	718	0.03	1.19

SA = calcite surface area.

assumed to be equal to one. The role of iteration was to consider successive dissolution and ex-solution of $CO_{2(g)}$ into and from the master solution, while keeping the total carbon moles in the system constant. These total carbon moles were made equal to those available in the system at each specific time interval. For instance, in the first step of iteration, the total carbon moles available in the system were assumed to be in the gas phase. In the second step, they were assumed to be in the solution. The $CO_{2(g)}$ fugacity in equilibrium was calculated on the basis of ΣCO_2. Carbon moles were then distributed between gas and solution phases. In the third step, another $CO_{2(g)}$ fugacity value in equilibrium was calculated on the basis of the new ΣCO_2 value. The $CO_{2(g)}$ fugacity values converged after 11 iterations. Results are shown in Table 1.

Activities and activity coefficients for Ca^{2+}, Cl^-, H^+, OH^-, and the carbonic acid components ($CO_{2(aq)}$, $HCO^-_{3\,(aq)}$, and $CO^{2-}_{3\,(aq)}$) were calculated using Pitzer's equations and the EQPITZ program (He and Morse, 1993). This program was used because the initial ionic strength of the master solution was high enough (~0.7 mol/L) to preclude the use of models more appropriate for dilute solutions (e.g., Debye-Huckel). Aqueous NH_4^+ was not taken into account by the EQPITZ program. Ammonium ion ($NH_4^+{}_{(aq)}$) may form ion pairs with both $HCO^-_{3\,(aq)}$ and $CO^{2-}_{3\,(aq)}$, thus reducing the activity of these species in solution. Pitzer (1991) showed that the activity coefficient for $NH_4^+{}_{(aq)}$ (γ_{NH4+}) may be approximated by $K^+{}_{(aq)}$ (γ_{K+}) for solutions similar in ionic strength to the master solution. Therefore, NH_4^+ was treated as K^+ for all calculations using the EQPITZ program. Further refinement of the solubility measurements would require interaction term data for $NH_4^+{}_{(aq)}$ which are not presently available in the literature. The activities of Ca-bearing complexes in the stock solution ($[CaOH]^+$, $[CaHCO_3]^+$, and $[CaCO_3]^0$) were calculated from the activities of

$Ca^{2+}_{(aq)}$, $OH^{-}_{(aq)}$, $HCO_3^{-}{}_{(aq)}$, and $CO_3^{2-}{}_{(aq)}$ using the equilibrium constants listed in Langmuir (1997). Results are shown in Table 1.

2.7. Saturation and Growth Rate

Saturation state with respect to a given mineral phase is defined as $\Omega = IAP/K_{sp}$, where IAP is the ionic activity product and K_{sp} is the solubility product for this particular mineral phase. Ionic activity products were calculated by multiplying the activity of $Ca^{2+}_{(aq)}$ and the activity of $CO_3^{2-}{}_{(aq)}$. Supersaturation with respect to calcite $\Omega_{calcite}$ was calculated using the EQPITZ program. An error of $\pm$ 9 U was estimated considering the error on the experimental measurements of Ca^{2+} ($\pm$0.006 mol/L). Supersaturation with respect to aragonite, vaterite, and monohydrocalcite was calculated by dividing IAP by the solubility product for aragonite (Plummer and Busenberg, 1982), for vaterite (Plummer and Busenberg, 1982), and for monohydrocalcite (Hull and Turnbull, 1973).

Calcite growth rate was calculated following the methodology described in Appendix 2 of Romanek et al. (1992). The cumulative sum of crystals nucleated over a given time interval was considered as seed material for subsequent overgrowth during an ensuing time interval. Growth rate was determined by dividing the precipitation rate over a specified time interval by the surface area of the cumulative seed material from previous time steps. Growth rates were calculated starting from the moment at which calcite (as rhombohedral-like forms in lysozyme-free or modified rhombohedral-like forms in lysozyme-bearing experiments) was the only mineral phase observed. These time intervals were over 3 h for the control experiments and the lysozyme-bearing experiments run at 0.1 mg/mL and 10 mg/mL, and over 6 h for the experiment run at 50 mg/mL of lysozyme. For the control experiment and for the lysozyme-bearing experiment run at 0.1 mg/mL of lysozyme, the cumulative surface area for calcite was determined using a geometric model that related mass to surface area for ideal calcite rhombs. Length and width of rhombs were measured in SEM pictures. The third dimension was estimated to be the average of the two visible dimensions. Particle surface area and volume were calculated as if the particles were rectangular prisms. For the experiments run at lysozyme concentrations of 10 and 50 mg/mL, cumulative surface area for calcite was determined using a geometrical model that related mass to surface area for ideal spheres. The radius of the sphere was measured in SEM pictures. In all calculations, calcite density was used to convert volume to mass, and surface area per gram was averaged for each grain.

3. RESULTS

3.1. Carbonate Precipitation Kinetics

Solution pH increased from 5.0 to 8.7 during a representative control experiment (lysozyme-free; Table 1, Fig. 2a). This increase occurred primarily within the first 1.5 h. Thereafter, increases in pH became slower and stabilized at 8.7. Overall trends in pH evolution were highly similar regardless of the presence or absence of lysozyme in solution (Fig. 2b). The presence of lysozyme, however, reduced the initial pH of the master solution down to one unit. From 3 h until the end of the experiment, pH values were almost identical for both lysozyme-free and lysozyme-bearing experiments.

For the control experiment, total calcium concentration in solution $Ca^{2+}{}_{T\ (aq)}$ decreased in ups and downs from an initial value of 0.25 mol/L to a value of 0.21 mol/L at 9 h (Table 1, Fig. 2a). This decrease was very fast within the first 1.5–2 h (from 0.25 mol/L to 0.22 mol/L). The $Ca^{2+}{}_{T(aq)}$ concentrations increased again, reaching a second maximum of 0.25 mol/L at 3 h. Afterwards, calcium concentrations in solution further decreased and stabilized at ~0.21 mol/L (Fig. 2a). Overall trends of $Ca^{2+}{}_{T(aq)}$ were quite similar in both lysozyme-free and lysozyme-bearing experiments (Fig. 2c). For instance, the first minimum occurred in both lysozyme-free and lysozyme-bearing experiments after ~1.5 h. Because $Ca^{2+}{}_{T(aq)}$ was not monitored continuously, absolute minima and maxima could not be unambiguously determined. On the other hand, final $Ca^{2+}{}_{T(aq)}$ concentrations became lower as lysozyme concentrations increased.

The presence of lysozyme in solution strongly affected the waiting time for precipitation (Fig. 2d). This time increased with the concentration of protein from 130 min for the lysozyme-free experiment to 6 h for lysozyme concentrations of 50 mg/mL. The number of crystals increased with protein concentration and crystal size decreased. For instance, the number of crystals (~200 crystals) for the experiment run at 50 mg/mL of lysozyme was twice that of the lysozyme-free experiment.

The saturation of the system with respect to calcite went up from 0 to ~2250 (in the control experiment), to ~2870 (lysozyme at 0.1 mg/mL), to ~2250 (lysozyme at 10 mg/mL), and to ~720 (lysozyme at 50 mg/mL) (Table 1). This increase took place primarily within the first 3.5 h for the control experiment and the one run at 10 mg/mL of lysozyme, within the first 4 h for the experiment run at 50 mg/mL of lysozyme, and within the first 5 h for the one run at 0.1 mg/mL of lysozyme (Fig. 2e). Thereafter, $\Omega_{calcite}$ stabilized at ~2290, ~2670, and at ~720 for the control, lysozyme 0.1 mg/mL, and 10 mg/mL experiments, respectively. For the experiment run at 50 mg/mL of lysozyme, the $\Omega_{calcite}$ values went down after 4 h. Crystals were first observed when $\Omega_{calcite}$ was ~1300 for the control experiment, ~900 for the experiment run at 0.1 mg/mL of lysozyme, ~1100 at 10 mg/mL of lysozyme, and ~1000 at 50 mg/mL of lysozyme (Fig. 2e).

Calcite growth rate varied from $10^{1.59}$ mol/m^{2}h to $10^{3.73}$ mol/m^{2}h for the control experiment, from $10^{1.91}$ mol/m^{2}h to $10^{2.91}$ mol/m^{2}h for a lysozyme concentration of 0.1 mg/mL, and from $10^{1.34}$ mol/m^{2}h to $10^{3.19}$ mol/m^{2}h for a concentration of 10 mg/mL. The growth rate was $10^{1.19}$ mol/m^{2}h at a lysozyme concentration of 50 mg/mL (Table 1). The presence of lysozyme in solution did not significantly affect the calcite growth rate, at least within the range 0 to 10 mg/mL (Fig. 2f).

3.2. The Evolution of Calcite Crystal Growth Morphology

Mainly spherulites were observed during the first stages of the control experiments. These spherulites later disappeared (at ~1 h after detection), thus giving rise to perfect rhombohedra. The same sequence was observed in lysozyme-bearing experiments. However, the transformation rate (spherulites to calcite crystals) became faster as lysozyme concentrations increased. No spherulites were observed in the experiment run at 50 mg/mL of lysozyme.

The effect of lysozyme–calcite interaction on the morphology of calcite crystals is illustrated in a morphogram (Fig. 3) in which a wide variety of morphologies can be observed at different times and for different protein concentrations. Crystals grown in the absence of protein (control samples) were always perfect rhombohedra of 60 to 80 μm in size after 24 h. At low protein concentration ($\leq$1 mg/mL) two of the edges of {104} faces (those not confluent to the ***c***-axis) were inhibited and new faces appeared. Inhibition always started at corners, where two of these edges meet. The new faces showed a terraced morphology with macro-steps. The symmetry of the

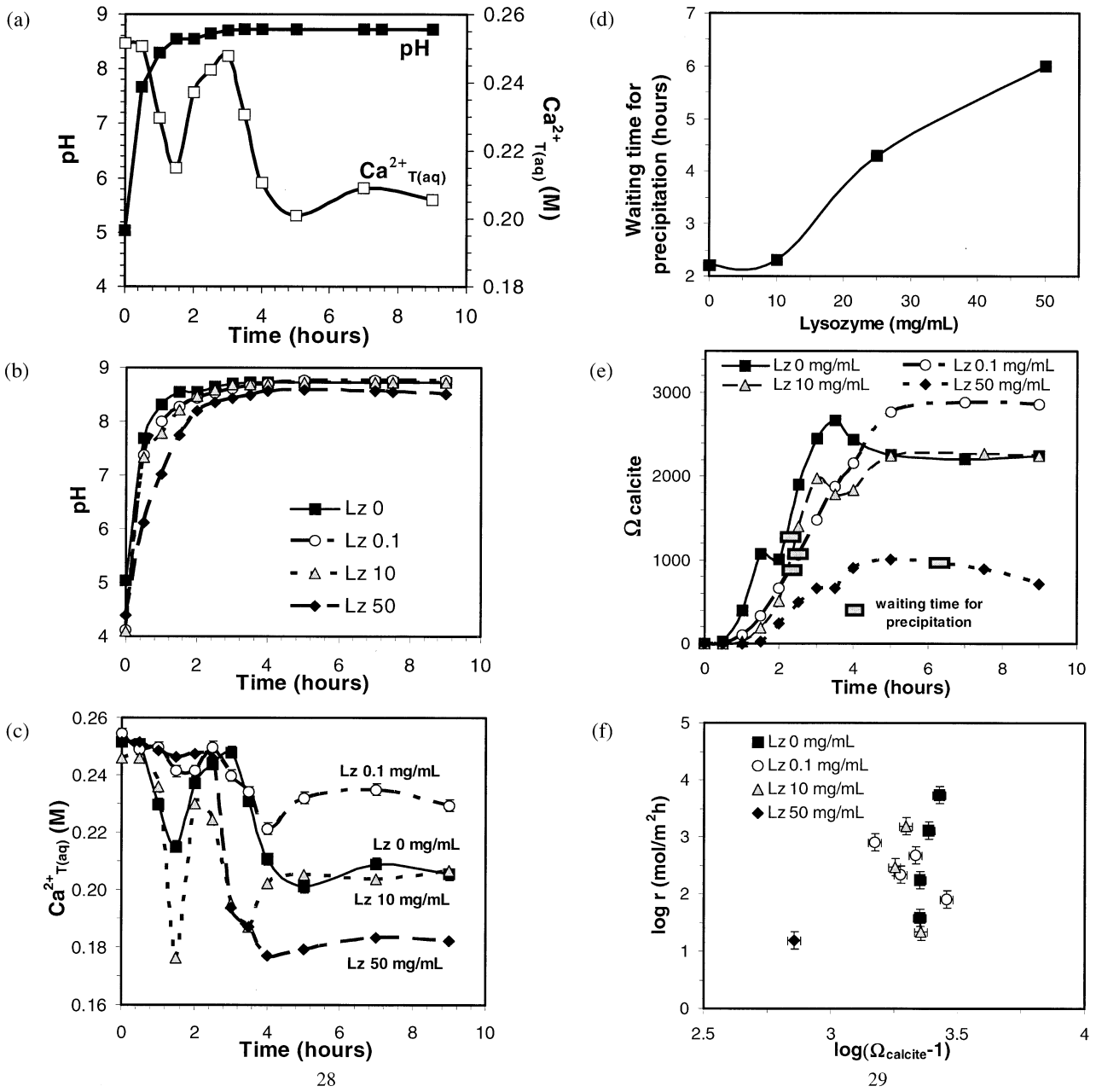

28 29

Fig. 2. Precipitation kinetics: (a) Measured pH and total aqueous calcium, $Ca^{2+}_{T\ (aq)}$ over time for the lysozyme-free experiment. (b) Measured pH of the master solution over time for lysozyme concentrations of 0, 0.1, 10, and 50 mg/mL. (c) Measured $Ca^{2+}_{T(aq)}$ over time for lysozyme concentrations of 0, 0.1, 10, and 50 mg/mL. (d) Waiting time for the precipitation as a function of lysozyme concentration. (e) Calculated supersaturation with respect to calcite over time for lysozyme concentrations of 0, 0.1, 10, and 50 mg/mL. The rectangles indicate $\Omega_{calcite}$ when the first solid was observed in the microbridges. (f) Instantaneous calcite growth rate as a function of $\Omega_{calcite}$ for lysozyme concentrations of 0, 0.1, 10, and 50 mg/mL. Data points at each lysozyme concentration correspond to different time intervals.

newly expressed faces corresponded to that of the {110} first-order prismatic form of calcite (Fig. 4a).

At an intermediate protein concentration (10 mg/mL), rhombohedral faces became smaller and second-order prismatic faces {100} were expressed in addition to the {110} faces (Fig. 4b). At a higher concentration (25 mg/mL), the growth of {001} faces was also inhibited and crystals exhibited only remnants of the {104} faces (Fig. 4c). At even higher lysozyme concentrations (50 mg/mL), calcite was inhibited in a nonspecific manner, resulting in the formation of spherical calcite aggregates. As growth progressed, sharp crystal edges in the calcite crystals composing these aggregates became rounded. The size of these crystals and that of the whole aggregate decreased with increasing protein concentrations. At lower protein concentrations, aggregates formed by crystals that were parallel to each other were occasionally observed (Fig. 4d).

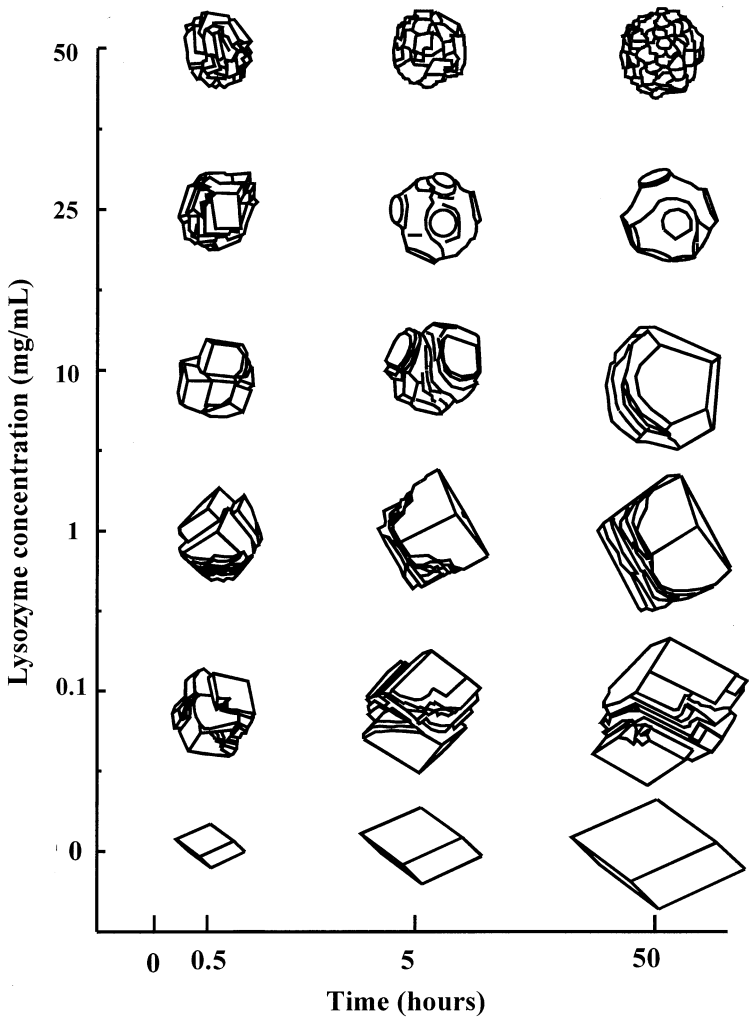

Fig. 3. Morphogram of calcite crystals grown at different lysozyme concentrations. Time is computed after the first calcite crystals were observed in the microbridges. The morphogram has been constructed from individual crystals and does not represent a time evolution of the morphology of the same crystal, but rather the most common morphologies of crystals collected at different times.

3.3. Overgrowth Calcite Crystals

Nucleation took place much earlier on calcite substrates (120 min at most) than in bulk solution (up to 6 h). During the initial stages (~120 min after closing the system), overgrowth calcite crystals were only observed on substrates at higher lysozyme concentrations (>10 mg/mL). At this time a few 3-D nuclei started to form at the edges of the rhombohedral faces of the calcite substrates. After 24 h, calcite 3-D nuclei covered all the faces of the calcite crystal substrate. Overgrowth crystals grew epitaxially since they displayed the same crystallographic orientation as the substrate. Interestingly, overgrowth crystals nucleated in lines which run diagonal to the rhombohedral faces of the substrate (Fig. 5). Parallel overgrowths were observed on all the {104} faces of the synthetic calcite substrate. The nucleation density of crystals on the substrate increases with protein concentrations (Fig. 5a–e). Each calcite crystal overgrown on the calcite substrates exhibited similar morphologies to those grown in the bulk solution but at higher lysozyme concentrations (about double).

4. DISCUSSION

4.1. Kinetics of Calcite Precipitation

Solution pH varies over time in the master solution due to the following factors: 1) $NH_{3(g)}$ dissolution, 2) $CO_{2(g)}$ dissolution, and 3) acid generation during carbonate formation (Jimenez-Lopez et al., 2001). The dissolution of $NH_{3(g)}$ in the $CaCl_2$ master solution contributed to an increase in the solution pH value following the equilibrium

$$NH_{3(g)} \Leftrightarrow NH_{3(aq)} \Leftrightarrow NH_{3(aq)} + H_2O \Leftrightarrow NH^+_4 + OH^-$$

Assuming the system approached chemical equilibrium, the dissolution of this $NH_{3(g)}$ requires that the pH of the master solution increase. As pH increases, $CO_{2(g)}$ hydrates to form $HCO^-_{3\,(aq)}$ and $CO^{2-}_{3\,(aq)}$ following the equilibrium

$$CO_{2(g)} + H_2O \Leftrightarrow H_2CO_{3(aq)} \Leftrightarrow HCO^-_{3(aq)} + H^+ \Leftrightarrow CO^{2-}_{3(aq)} + H^+$$

Finally, the precipitation of solid carbonate liberates H^+, thus

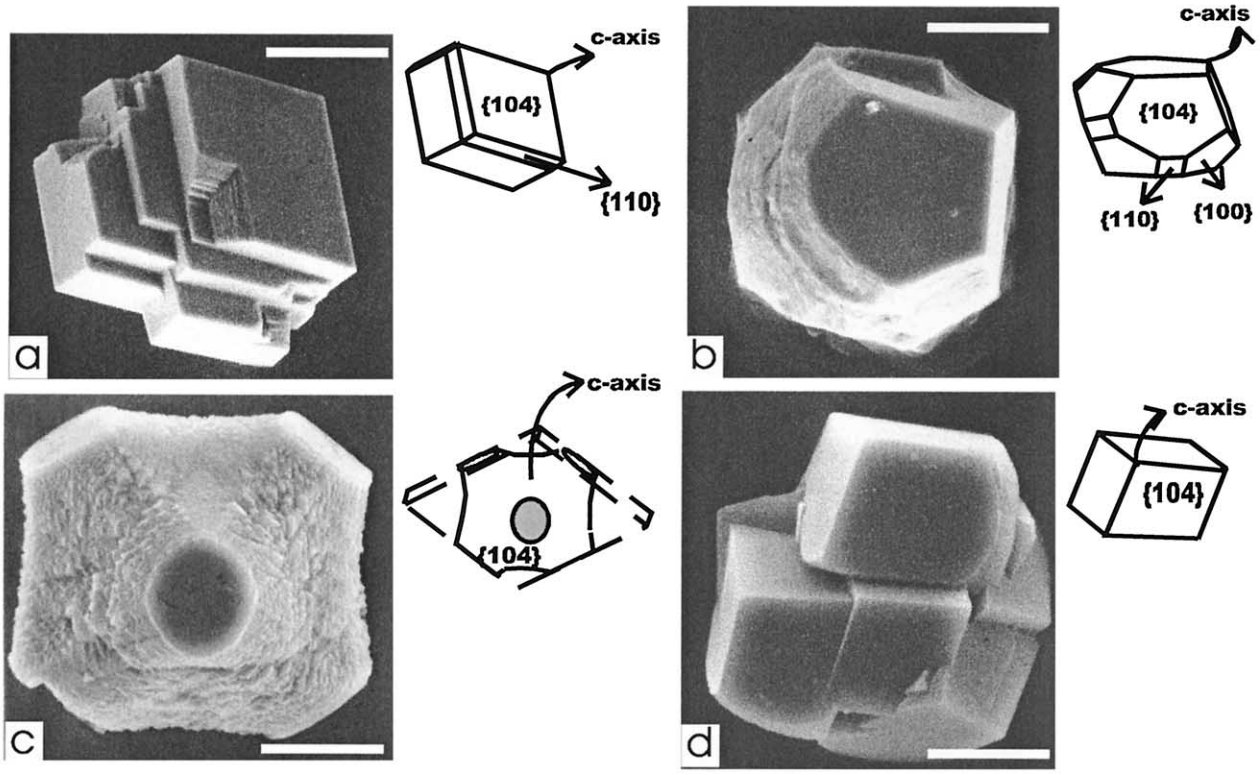

Fig. 4. SEM images and face indexes of calcite crystals grown in the presence of lysozyme at different concentrations: (a) Calcite crystal collected after 50 h showing small {110} faces (lysozyme concentration = 0.1 mg/mL); (b) calcite crystal collected after 50 h showing {110} and {101} faces (lysozyme concentration = 10 mg/mL); (c) calcite crystal collected after 50 h showing only the remnant of {104} faces (lysozyme concentration = 25 mg/mL); and (d) aggregate of rhombohedral calcite crystals formed at the initial stages of growth (lysozyme concentration = 10 mg/mL). Scale bars are 20 μm.

decreasing the pH of the master solution. The sharp increase of pH in the master solution during the first 0.5 h (Fig. 2a) can be accounted for by a significant incorporation and hydration of $NH_{3(g)}$. The three processes compete thereafter, resulting in a relative stabilization of the solution pH.

The evolution of calcium ions in solution was directly related to the precipitation and dissolution of calcium carbonate. The first minimum observed in $Ca^{2+}{}_{T(aq)}$ at 1.5 to 2 h (Fig. 2a) was induced by the precipitation of a calcium carbonate phase (either amorphous calcium carbonate or a metastable calcium carbonate phase). This metastable phase was crystalline according to observations with polarized light. However, this phase could not be characterized by X-ray diffraction because the amount of sample collected from the microbridges was insufficient for such analyses. Thermodynamic/speciation calculations based on the aqueous species present in the system ($Ca^{2+}{}_{(aq)}$, $Cl^{-}{}_{(aq)}$, $CO_{3(aq)}$, $HCO_3^{-}{}_{(aq)}$, $CO_3^{2-}{}_{(aq)}$, $H^{+}{}_{(aq)}$, $OH^{-}{}_{(aq)}$, $(CaHCO_3)^{+}{}_{(aq)}$, $(CaCO_3)^{0}{}_{(aq)}$ and $(CaOH)^{+}{}_{(aq)}$) showed that during the first stages of the experiment: 1) the master solution was supersaturated with respect to aragonite, vaterite, and monohydrocalcite, thus thermodynamically stabilizing the precipitation of any one of these phases; and 2) calcium in solution was mainly in the form of $Ca^{2+}{}_{(aq)}$, exceeding all other forms of Ca-species (Table 1). The characteristic needle-like forms of aragonite were not detected. Instead, the first mineral phase detected was that of spherulites, which could correspond to vaterite or monohydrocalcite. Formation of spherulites of vaterite and monohydrocalcite during the precipitation of calcium carbonate has previously been observed by Ogino et al. (1987) and Jimenez-Lopez et al. (2001), respectively. The authors observed the precipitation of these phases and their later dissolution, giving rise to calcite. On the other hand, the predominance of $Ca^{2+}{}_{(aq)}$ in the master solution may induce the preferential precipitation of the hydrous phase (monohydrocalcite) over the anhydrous ones (i.e., vaterite, aragonite, or calcite). Hydrated Ca^{2+} must shed its hydration sphere in the adsorption layer (solid–solution interface) and must then dissociate its last water molecule before it can be incorporated into the anhydrous crystal lattice (Lippmann, 1973). The precipitation of monohydrocalcite may be kinetically favored with respect to the anhydrous phases, because the energy necessary to dehydrate Ca^{2+} does not have to be overcome (Lippmann, 1973). It is then possible that the metastable phase observed in our experiments was monohydrocalcite. An unambiguous characterization could not, however, be done.

The precipitation of this first phase removed calcium from the solution, favoring the formation of the stable phase (calcite) and triggering the competition of these two phases. The increase in $Ca^{2+}{}_{T(aq)}$ concentration within the 2- to 3-h interval (Fig. 2a) was brought about by the dissolution of this first metastable calcium carbonate phase, which dissolved at a faster

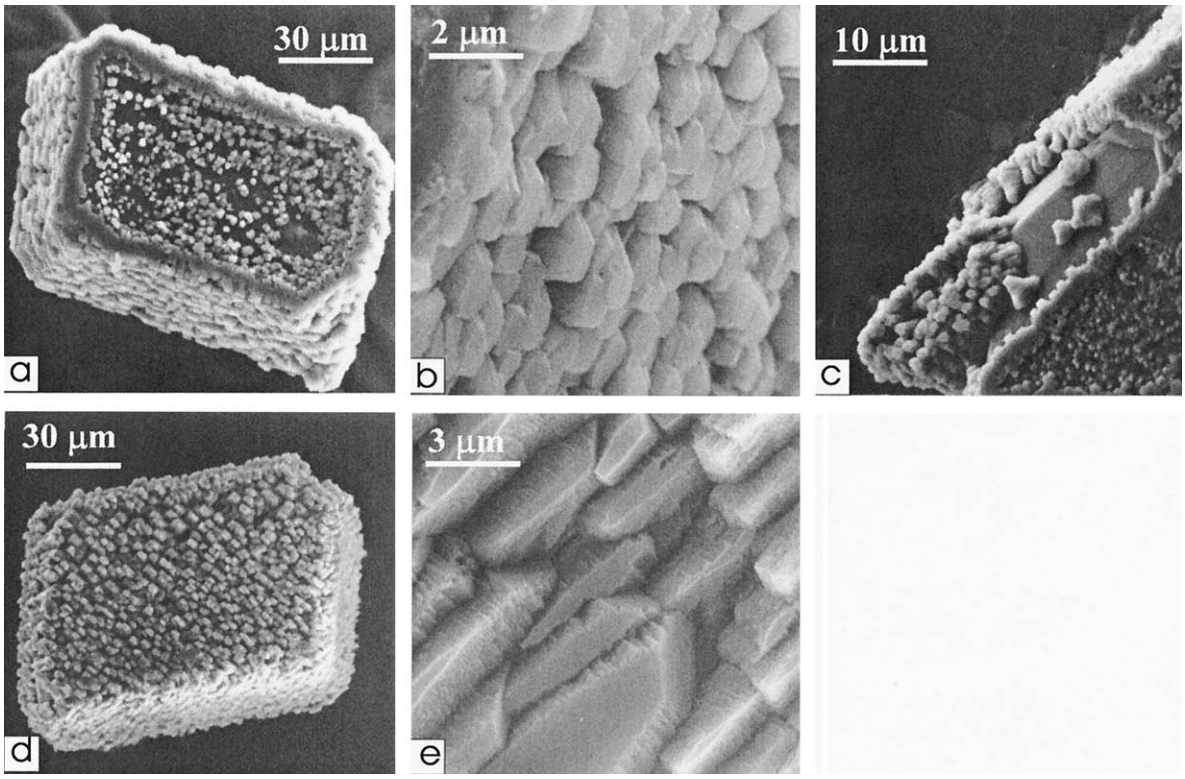

Fig. 5. Overgrown rhombohedral calcite crystals in the presence of lysozyme at different protein concentrations in the master solution: (a) lysozyme concentration = 10 mg/mL; (b) lysozyme concentration = 10 mg/mL (detail of overgrowth crystals shown in Fig. 5a); (c) lysozyme concentration = 10 mg/mL (detail of the overgrown crystal shown in Fig. 5a). The detail shows one edge of the overgrown crystal where the surface of the crystal seed is observed; (d) lysozyme concentration = 25 mg/mL; and (e) lysozyme concentration = 25 mg/mL (detail of overgrowth crystals shown in Fig. 5d).

rate than the calcite formation. The subsequent decrease in $Ca^{2+}{}_{T(aq)}$ after ~3 h was due exclusively to calcite precipitation, because the characteristic rhombohedral calcite crystals were the only forms observed. The sequential precipitation of a metastable form of calcium carbonate, which later dissolved giving rise to calcite, is consistent with the Ostwald Step Rule described by Morse and Casey (1988).

The first $Ca^{2+}{}_{T(aq)}$ minimum (at 1.5 h) occurred at the same time in both lysozyme-free and lysozyme-bearing experiments (Fig. 2c). This observation suggested that the precipitation of the first metastable calcium carbonate phase took place regardless of the presence or absence of lysozyme. The time at which the first $Ca^{2+}{}_{T(aq)}$ minimum occurred was very close to that at which the first precipitate was observed (~2 h; Fig. 2d) in lysozyme-free and lysozyme-bearing experiments at low lysozyme concentrations (≤10 mg/mL). However, at higher concentrations (50 mg/mL), the delay between these two times extended to ~4 h (Figs. 2c and 2d). The experimentally determined waiting time for precipitation (at which the first crystals were detected) is the sum of: 1) induction time and 2) observation time. Induction time, which is of kinetic nature, is the time required for the clusters to reach a critical size and thus to become stable. Observation time is that required for the nucleus to reach a size that can be detected using an optical microscope (Garside, 1981). The delay in the waiting time for precipitation with respect to the first $Ca^{2+}{}_{T(aq)}$ minimum, at a lysozyme concentration of 50 mg/mL, was not caused by inhibition of the formation of the metastable calcium carbonate phase (there was a slight decrease in $Ca^{2+}{}_{T(aq)}$ at ~1.5 h). It is however probably caused by the small size of crystals, which made it difficult to observe them using an optical microscope.

At the time of metastable phase precipitation (~1.5 h) and calcite precipitation (~3 h), the values of $\Omega_{calcite}$ decreased with increasing protein concentrations (Fig. 2e). This observation suggests that lysozyme favored the nucleation of both the metastable phase and calcite, thus enabling nucleation at lower values of supersaturation. This observation also agrees with the increase in the number of crystals detected as protein concentrations increase, which could indicate a more intense nucleation. Proteins in solution locally raise Ca^{2+} concentrations in those regions close to negatively charged patches on the protein surface (ionotropic effect; Addadi et al., 1987; Addadi and Weiner, 1992). This creates local areas with higher saturation values than those of the bulk solution. Nucleation would be favored in those areas, although saturation in the bulk solution is not high enough to produce nucleation. This, however, did not affect the calcite growth rate, at least at low lysozyme concentrations (0.1 to 10 mg/mL).

4.2. Morphology of Calcite Crystals

Modifications in crystal growth (Addadi and Weiner, 1992) and dissolution behavior (Teng and Dove, 1997) can provide insights regarding proteins–mineral surface interactions. For

Table 2. Density of carbonates on calcite faces and orientation of carbonate groups with respect to calcite surface. The faces are sorted in the same sequence as they were affected by their interaction with the protein.

Face	Density (nm^{-2})	Orientation
{110}	5.72	90°
{100}	2.35	90°
{001}	4.64	0°
{104}	4.95	44.6°

instance, in both cases modification of the habit of calcite crystals is induced by the preferential adsorption of proteins to specific faces which are expressed as a consequence of reductions in their growth (or dissolution) rate. In a previous study it was observed (Rodriguez-Navarro et al., 2000) that the interaction between globular proteins (e.g., lysozyme) and calcite surfaces mainly depends on the surface charge of the protein and the crystal surface. The effect of proteins in the final morphology of calcite crystals depends on the nature of the protein charge (Rodriguez-Navarro et al., 2000). Negative proteins preferentially interact with {110} calcite surfaces, this interaction becoming more pronounced as the protein is more negatively charged. Lysozyme is positively charged (at the pH of calcite precipitation ~8.7) and yet interacts preferentially with {110} calcite faces. The affinity of lysozyme for these faces is, however, lower compared to that of negatively charged proteins. This indicates that, in addition to electrostatic interaction, other factors probably intervene in the adsorption of proteins onto crystal faces.

One possibility is that lysozyme functional groups interact more directly with calcite surfaces at the atomic level. However, lysozyme size is quite large (~30 Å), a factor of >4 times greater than the distances between carbonate groups (or calcium) in the calcite faces (4 to 8 Å). The packing of these protein molecules cannot match the arrangement of sites on the calcite faces at the atomic level, and it is therefore difficult to maintain that geometrical matching at atomic scale exists.

Another possibility is that interaction between proteins and calcite faces may also be determined by the orientation of carbonate groups in calcite surfaces. Proteins preferentially interact with those faces where carbonate groups are perpendicular to the surface, e.g., such crystal faces running parallel to the calcite ***c***-axis as the {110} and {100} faces (Addadi et al., 1987; Mann et al., 1990). Our experiments showed that lysozyme interacted preferentially with {110} faces, which have the maximum density of carbonate groups and in which the carbonate groups are oriented perpendicular to the surface (Table 2). Once the {110} faces were covered, lysozyme interacted with the {100} faces, in which the carbonate groups are also oriented perpendicular to the surface although the density of carbonate groups is lower (Table 2). Finally, lysozyme interacted with the {001} faces, which have a high carbonate density, although the orientation of carbonate groups is parallel to the surface. Thus the sequential inhibition of the growth of the {110}, {100}, and {001} faces could be caused by the combined effect of the density of carbonate groups and their orientation.

4.3. Overgrowth of Calcite Crystals

In the absence of proteins, epitaxial growth of calcite on calcite crystals takes place through the screw dislocation mechanism or two-dimensional nucleation (Gratz and Hillner, 1993). Our results showed that the overgrowth of calcite crystals occurred in the presence of lysozyme through the deposition of isolated 3-D clusters (Fig. 5). Overgrown crystals displayed the same crystallographic orientation as the substrate (the {104} face) and were arranged in lines running diagonal to the rhombohedral faces of the substrate. It should be noted that these lines fit the orientation of the carbonate groups in the rhombohedral faces of the calcite substrate. Crystallites form preferentially near the corner and edges of the calcite crystal substrate (Fig. 5a). It is known that during crystal growth, particularly when the growth mechanism is dominated by transport diffusion in the bulk, the supersaturation is greater near the edges than in the center of the faces, favoring the nucleation on this particular locations (Berg, 1938).

Our results also showed that lysozyme favored and controlled heterogeneous nucleation of calcite on the calcite substrate. In the presence of lysozyme, the nucleation on calcite substrates occurred significantly earlier than in the bulk solution. The reason for the enhancement of the nucleation may be that an adsorption layer of protein forms on calcite surfaces (Aizenberg et al., 1994; Teng and Dove, 1997). In fact, it is known that near the surface there is an increase in protein concentrations that changes the activity of the solution close to the crystal face (Norde and Lyklema, 1991). This leads to a decrease in the surface energy, which in turn reduces the nucleation barrier. Furthermore, the stacking of the overgrowth 3-D calcite crystallites (Fig. 5b) leaves gaps in which the protein is occluded. This 3-D nucleation mechanism may account for the high quantities of proteins observed in many biomineral structures (Nys et al., 1999) including those that still behave like a single crystal (Berman et al., 1990; Aizenberg et al., 1997). In summary, the calcite blocks could nucleate on top of each other with a parallel orientation, thus leaving gaps that are filled with proteins. The resulting polycrystalline aggregate still preserves a crystallographic continuity and, at the same time, incorporates a substantial amount of organic matter.

5. CONCLUSIONS

Free-drift calcite precipitation experiments were conducted in the presence of lysozyme to examine the effects of the protein on the precipitation kinetics of calcium carbonate and on calcite crystal morphology. Nucleation and growth of calcium carbonate crystals were primarily driven by the dissolution of $NH_{3(g)}$ into the reacting solution from an underlying reservoir of ammonium bicarbonate (NH_4HCO_3). Calcium was removed through the precipitation of solid carbonate, and pH was buffered by the hydrolysis of ammonia gas.

Regardless of the presence of lysozyme, calcite precipitation was preceded by the precipitation of a metastable phase. With increasing concentration of lysozyme, the precipitation of the metastable phase occurred at lower values of $\Omega_{calcite}$. Afterwards, the metastable phase dissolved and then gave rise to calcite as the sole solid phase. Also, with increasing concentrations of lysozyme, calcite nucleation took place at lower

values of $\Omega_{calcite}$. Calcite growth rate was not affected at low concentrations of lysozyme ($\leq$10 mg/mL).

The presence of lysozyme drastically modified the morphology of calcite crystals, which preferentially interacted with faces parallel to the **c**-axis. The growth of {110}, {100}, and finally {001} faces was sequentially inhibited at increasing lysozyme concentrations. Presumably, the {110} faces became completely covered by the protein as lysozyme concentrations increased. Other faces ({100} and {001}) of decreasing affinities then competed for protein adsorption. Varying affinities for calcite crystallographic faces may be caused by differences in their surface charge density and in the orientation of carbonate groups. The overgrowth of calcite crystals occurred in the presence of lysozyme through the deposition of isolated 3-D blocks, and it is this mechanism which may explain the occlusion of large quantities of protein into biomineral structures which maintain their crystallographic coherence.

Acknowledgments—We are grateful to the Spanish Ministerio de Educación y Ciencia for financial support through the Picasso Program and the EU project "European Bio-Crystallogenesis Initiative" (BIO4-CT98-0086). We would like to thank Prof. Christopher Romanek, Prof. Yves Nys, Dr. David E. Cole, and two anonymous reviewers for their valuable comments. Thanks also to Marco Bettini for the English editing.

Associate editor: D. Cole

REFERENCES

Addadi L., Moradian J., Shay E., Maroudas N. G., and Weiner S. (1987) A chemical model for the cooperation of sulfates and carboxylates in calcite crystals formation. *Proc. Natl. Acad. Sci. USA* **84,** 2732–2736.

Addadi L. and Weiner S. (1992) Control and design principles in biological mineralization. *Angew. Chem. Int. Ed. Engl.* **31,** 153–169.

Aizenberg J., Albeck S., Weiner S., and Addadi L. (1994) Crystal proteins interactions studied by overgrowth of calcite on biogenic skeletal elements. *J. Crys. Growth* **142,** 156–164.

Aizenberg J., Hanson J., Koetzle T. F., Weiner S., and Addadi L. (1997) Control of macromolecule distribution within synthetic and biogenic single. *J. Am. Chem. Soc.* **119,** 881–886.

Arai T. and Norde W. (1990) The behaviour of some model proteins at solid-liquid interfaces: Adsorption from single proteins solutions. *Colloids and Surfaces* **51,** 1–15.

Belcher A. M., Wu X. H., Christensen R. J., Hansma J., Stucky G. D., and Morse D. E. (1996) Control of crystal phase switching and orientation by soluble mollusc-shell proteins. *Nature* **381,** 56–58.

Berg W. F. (1938) Proc. *Roy. Soc.* **A164,** 79.

Berman A., Addadi L., Kvick A., Leiserowitz L., Nelson M., and Weiner S. (1990) Intercalation of sea-urchin proteins in calcite-study of a crystalline-composite material. *Science* **250,** 664–667.

Checa A. and Rodriguez-Navarro A. (2001) Geometric and crystallographic constraints determining the self-organisation of shell microstructures in Unionidae (Bivalvia, Mollusca). *Proc. Roy. Soc. London B* **250,** 771–778.

Falini G., Albeck S., Weiner S., and Addadi L. (1995) Control of aragonite or calcite polymorphism by Mollusk shell macromolecules. *Science* **271,** 67–69.

Garside J. (1981) Nucleation. In *Biological Mineralization and Demineralization* (ed. G. H. Nancollas), Life Sciences Research Report 23, pp. 23-35. Springer-Verlag.

Gratz A. J. and Hillner P. E. (1993) Poisoning of calcite growth viewed in the atomic force microscope (AFM). *J. Crys. Growth* **129,** 789–793.

Haynes C. A. and Norde W. (1994) Globular proteins at solid/liquid interfaces. *Colloids and Surfaces B: Biointerfaces* **2,** 517–566.

He S. and Morse J. W. (1993) The carbonic acid system and calcite solubility in aqueous Na-K-Ca-Mg-Cl-SO_4 solutions from 0 to 90°C. *Geochim. Cosmochim. Acta* **57,** 3533–3554.

Heywood B. R. (1996) Templated-directed nucleation and growth of inorganic materials. In *Biomimetic Materials Chemistry* (ed. S. Mann), pp. 143–173. VCH, New York.

Hull H. and Turnbull A. G. (1973) A thermochemical study of monohydrocalcite. *Geochim. Cosmochim. Acta* **37,** 685–694.

Jimenez-Lopez C., Caballero E., Huertas F. J., and Romanek C. S. (2001) Chemical, mineralogical and isotopic behavior and phase transformation during the precipitation of calcium carbonate minerals from intermediate ionic solution at 25°C. *Geochim. Cosmochim. Acta* **65**(19), 3219–3231.

Langmuir D. (1997) *Aqueous Environmental Chemistry*. Prentice Hall, New York. 600 pp 194–229.

Lippmann F. (1973) Sedimentary carbonate minerals. In *Mineral, Rocks and Inorganic Materials*. von Engelhardt W., Hahn T., Roy R., and Wyllie P. J., eds. Springer-Verlag, Berlin. 228 pp.

Lowenstand H. A. (1981) Minerals formed by organisms. *Science* **211,** 1126–1131.

Lowenstand H. A. and Weiner S. (1989) *On Biomineralization*. Oxford University Press, New York.

Mann S. (1988) Molecular recognition in biomineralization. *Nature* **332,** 119–124.

Mann S., Webb J., and Williams R. J. P. (1989) *Biomineralization, Chemical and Biochemical Perspectives.* VCH, Weinheim.

Mann S., Didymus J. M., Sanderson N. P., and Heywood B. R. (1990) Morphological influence of functionalised α, ω-dicarboxylates on calcite crystallization. *J. Chem. Soc. Faraday Trans.* **86,** 1873–1880.

Morse J. W. and Casey W. H. (1988) Ostwald processes and mineral paragenesis in sediments. *Am. J. Sci.* **288,** 537–560.

Morse J. W. and Mackenzie F. T. (1990) *Geochemistry of Sedimentary Carbonates*. Elsevier, New York. 426 pp 1–19.

Norde W. and Lyklema J. (1991) Why proteins prefer interfaces? *J. Biomater. Sci. Polymer Edn.* **2,** 183–202.

Nys Y., Hincke M. T., Arias J. L., Garcia-Ruiz J. M., and Solomon S. E. (1999) Avian eggshell mineralization. *Poultry Avian Biol. Rev.* **10,** 143–166.

Ogino T., Suzuki T., and Sawada K. (1987) The formation and transformation mechanism of calcium carbonate in water. *Geochim. Cosmochim. Acta* **51,** 2757–2767.

Pitzer K. S. (1991) *Activity Coefficients in Electrolyte Solutions*. CRC Press, Boca Raton, Florida. 542 pp 414–419.

Plummer L. N. and Busenberg E. (1982) The solubility of calcite, aragonite and vaterite in CO_2-water solutions between 0–90°C and a evaluation of the aqueous model for the system CO_2-H_2O-$CaCO_3$. *Geochim. Cosmochim. Acta* **46,** 1011–1040.

Rodriguez-Navarro A., Messier R., Jimenez-Lopez C., and Garcia-Ruiz J. M. (2000) Importance of electrostatic interactions between calcite surfaces and proteins. *Mat. Res. Soc. Symp. Proc.* **599,** 353–359.

Romanek C., Grossman E., and Morse J. (1992) Carbon isotopic fractionation in synthetic calcite, effects of temperature and precipitation rate. *Geochim. Cosmochim. Acta* **56,** 419–430.

Simkiss K. and Wilbur K. M. (1989) *Biomineralization: Cell Biology and Mineral Deposition*. Academic Press, San Diego.

Teng H. H. and Dove P. M. (1997) Surface site-specific interactions of aspartate with calcite during dissolution: Implication for biomineralization. *Am. Mineral.* **82,** 878–887.

Wheeler A. P., George J. W., and Evans C. A. (1981) Control of calcium carbonate nucleation and growth by soluble matrix of oyster shell. *Science* **212,** 1397–1398.

Wolery T. J. (1992) EQ3/6, a software package for geochemical modeling of aqueous systems, version 7. 0. Lawrence Livermore National Laboratory, University of California, Livermore.